

Triplet superconductivity in a 1D itinerant electron system with transverse spin anisotropy

C. Dziurzik¹, G.I. Japaridze^{2,a}, A. Schadschneider^{1,b}, I. Titvinidze^{3,a,c}, and J. Zittartz¹

¹ Institut für Theoretische Physik, Universität zu Köln, 50937 Köln, Germany

² Max-Planck-Institut für Physik komplexer Systeme, Nöthnitzer Str. 38, 01187 Dresden, Germany

³ Institut für Theorie der Kondensierten Materie Universität Karlsruhe, 76128 Karlsruhe, Germany

Received 31 October 2005 / Received in final form 24 February 2006

Published online 31 May 2006 – © EDP Sciences, Società Italiana di Fisica, Springer-Verlag 2006

Abstract. In this paper we study the ground state phase diagram of a one-dimensional $t-J-U$ model away from half-filling. In the large-bandwidth limit and for ferromagnetic exchange with easy-plane anisotropy a phase with gapless charge and massive spin excitations, characterized by the coexistence of triplet superconducting and spin density wave instabilities is realized in the ground state. With increasing ferromagnetic exchange transitions into a ferrometallic and then a spin gapped triplet superconducting phase take place.

PACS. 71.10.Hf Non-Fermi-liquid ground states, electron phase diagrams and phase transitions in model systems – 71.10.Fd Lattice fermion models (Hubbard model, etc.) – 74.20.Mn Unconventional mechanisms (spin fluctuations, polarons and bipolarons, resonating valence bond model, anyon mechanism, marginal Fermi liquid, Luttinger liquid, etc.) – 71.27.+a Strongly correlated electron systems; heavy fermions

1 Introduction

Experimental and theoretical investigations show that many strongly correlated electronic systems exhibit surprisingly complex phase diagrams [1]. Especially the competition or coexistence of magnetic order and superconductivity is a topic of increased current interest. Magnetically mediated Cooper pairing near the antiferromagnetic instability is widely discussed in the context of superconductivity in copper-oxide systems [2,3]. Moreover, the discovery of Triplet Superconductivity (TS) in Sr_2RuO_4 [4] and the recent discovery of coexistence of the TS phase with ferromagnetism in UGe_2 [5], URhGe [6] and ZrZn_2 [7] has triggered an increased activity in studies of correlated electron models showing close proximity of triplet superconducting and ferromagnetically ordered phases [8–17].

Another challenging problem is superconductivity in quasi-one-dimensional compounds [19]. More than two decades have passed since the discovery of superconductivity in so-called Bechgaard salts such as $(\text{TMTSF})_2\text{X}$ with $\text{X} = \text{PF}_6, \text{ClO}_4$, etc. [20]. Most interesting is the phase diagram of $(\text{TMTSF})_2\text{PF}_6$ which shows a spin-Peierls (SP) phase in the ground state at atmospheric pressure. In-

creasing pressure leads first to a transition from the SP phase into a spin density wave (SDW) phase, and finally to the suppression of the SDW ground state in favor of superconductivity [21]. In last years an increasing amount of convincing experimental evidence has been accumulated in favour of the triplet superconducting ordering in these compounds [22]. This triggered interest in low-dimensional models of correlated electrons showing mechanism for Cooper pairing of triplet symmetry coexisting or closely competing with SDW type ordering. Although a wide variety of theoretical approaches have so far been used to study this topic [23–29], the understanding of the microscopic mechanisms for the complex phenomena in these compounds is still far from complete.

In [30] an extension of the Hubbard model including anisotropic spin-spin interactions has been proposed as a suitable model for systems with coexisting orders. The model describes a system of itinerant electrons with anisotropic spin-exchange interaction between electrons on nearest-neighbor sites. The one-dimensional version of the Hamiltonian reads:

$$\mathcal{H} = -t \sum_{n,\alpha} (c_{n,\alpha}^\dagger c_{n+1,\alpha} + c_{n+1,\alpha}^\dagger c_{n,\alpha}) + U \sum_n \rho_{n,\uparrow} \rho_{n,\downarrow} + \frac{J_{xy}}{2} \sum_n (S_n^+ S_{n+1}^- + h.c.) + J_z \sum_n S_n^z S_{n+1}^z. \quad (1)$$

Here $c_{n,\alpha}^\dagger$ ($c_{n,\alpha}$) is the creation (annihilation) operator for an electron at site n with spin α , $\rho_\alpha(n) = c_{n,\alpha}^\dagger c_{n,\alpha}$, $\mathbf{S}(n) = \frac{1}{2} c_{n,\alpha}^\dagger \boldsymbol{\sigma}_{\alpha\beta} c_{n,\beta}$ where σ^i ($i = x, y, z$) are the Pauli matrices.

^a Permanent address: Andronikashvili Institute of Physics, Georgian Academy of Sciences, Tamarashvili 6, Tbilisi 0177, Tbilisi, Georgia.

^b e-mail: as@thp.uni-koeln.de

^c Current address: Institut für Theoretische Physik, J.W. Goethe-Universität Frankfurt, Max-von-Laue-Str. 1, 60438 Frankfurt/Main, Germany

Indeed, this model was shown to exhibit an extremely rich phase diagram in the case of a half-filled band [30,31]. In particular in the case of the ferromagnetic XY-type exchange interactions the ground state phase diagram consists of sequence of transitions (with increasing ferro exchange) from a metallic phase with coexisting TS^0 and SDW^z instabilities, into an insulating Néel type antiferromagnetic phase and finally, for strong XY-type ferro-exchange into the insulating *ferromagnetic* XY phase [31].

In this paper we study the *effect of doping* on the ground state phase diagram of the model (1). We use a combined approach based on continuum-limit bosonization and DMRG techniques. In the range of applicability of the continuum-limit approach we have obtained the ground state phase diagram for a wide range of model parameters and band-fillings ν . In our numerical studies we restrict our consideration to the case of a quarter-filled band with XY-type spin exchange interaction and on-site repulsion $U \geq 0$. We investigate the excitation spectrum of the system as well as the behavior of various correlation functions. Depending on the relation between the model parameters J_{xy}/t and U/t we have shown the existence of four different metallic phases in the ground state (see Fig. 10): in the case of antiferromagnetic exchange the system shows properties of a spin gapped (Luther-Emery) metal with coexistence of the singlet-superconducting and charge-density-wave (CDW) instabilities. The line $J_{xy} = 0$ corresponds to the Luttinger Liquid phase and marks the transition from a spin gapped sector with singlet Cooper pairing (antiferromagnetic exchange) into the spin gapped sector with triplet Cooper pairing (ferromagnetic exchange). For weak ferromagnetic exchange, at $J_{xy}^c < J_{xy} < 0$ the system displays properties of a spin gapped metal with coexistence of the triplet superconducting and spin-density-wave (SDW^z) instabilities. For ferromagnetic spin coupling the spin gap dependence on strength of the transverse exchange exhibits a dome-type shape, opening at $J_{xy} = 0$ and closing at $J_{xy} = J_{xy}^c$. At $J_{xy} < J_{xy}^c$ a rather unconventional ferrometallic phase with gapless spin excitations and strongly dominating transverse ferromagnetic and triplet superconducting instabilities in the ground state is observed. Finally, at $J_{xy} < J_{xy}^c$, our numerical data indicates on opening of the spin gap. In this phase the system is expected to show properties of a triplet superconductor.

The paper is organized as follows: in the next section the weak-coupling continuum-limit version of the model is investigated. This allows to derive the weak-coupling phase diagram (Sect. 3). In Section 4 results of DMRG studies for chains up to $L = 120$ sites are presented. Finally, Section 5 is devoted to a discussion and concluding remarks.

2 Continuum-limit bosonization

Below in this section we consider the low-energy effective field theory of the model (1) in the case of non-half-filled band.

The standard bosonization procedure allows to express the initial lattice model in terms of two independent bosonic Hamiltonians

$$\mathcal{H} = \mathcal{H}_c + \mathcal{H}_s$$

describing respectively the *charge* (c) and *spin* (s) degrees of freedom. For the band-filling $\nu \neq 1/2$, the gapless charge sector is described by the free Bose field Hamiltonian

$$H_c = \frac{v_c}{2} \int dx \left\{ \frac{1}{K_c} (\partial_x \varphi_c)^2 + K_c (\partial_x \vartheta_c)^2 \right\}, \quad (2)$$

while the spin sector is governed by the quantum Sine-Gordon field

$$H_s = \frac{v_s}{2} \int dx \left\{ \frac{1}{K_s} (\partial_x \varphi_s)^2 + K_s (\partial_x \vartheta_s)^2 + \frac{2m_s}{a_0^2} \cos(\sqrt{8\pi} \varphi_s) \right\}. \quad (3)$$

Here $\varphi_{c,s}(x)$ and $\vartheta_{c,s}(x)$ are mutually dual bosonic fields

$$[\varphi_{c,s}(x), \vartheta_{c,s}(x)] = \frac{i}{2},$$

$$\partial_t \varphi_{c,s} = v_{c,(s)} \partial_x \vartheta_{c,s}, \quad \partial_x \varphi_{c,s} = \frac{1}{v_{c,(s)}} \partial_t \vartheta_{c,s}, \quad (4)$$

and a_0 is the infrared cutoff of the theory. The model parameters are given by

$$2(K_c - 1) \equiv g_{0c} = -\frac{1}{\pi v_F} \left[U - (J_{xy} + \frac{1}{2} J_z) \cos(2\pi\nu) \right], \quad (5)$$

$$2(K_s - 1) \equiv g_{0s} = \frac{1}{\pi v_F} \left[U - J_z - (J_{xy} - \frac{J_z}{2}) \cos(2\pi\nu) \right], \quad (6)$$

$$2\pi m_s \equiv g_{\perp} = \frac{1}{\pi v_F} \left[U - J_{xy} - \frac{J_z}{2} \cos(2\pi\nu) \right] \quad (7)$$

and the velocities of charge and spin excitations $v_{c,(s)} = v_F/K_{c,(s)}$, where $v_F = 2ta_0 \sin(\pi\nu)$.

Since at $\nu \neq 1/2$ the charge sector is described by the free Gaussian field (2) the vacuum averages of exponentials of the charge fields show a power-law decay at large distances

$$\langle e^{i\sqrt{2\pi}\varphi_c(x)} e^{-i\sqrt{2\pi}\varphi_c(x')} \rangle \sim |x - x'|^{-K_c}, \quad (8)$$

$$\langle e^{i\sqrt{2\pi}\vartheta_c(x)} e^{-i\sqrt{2\pi}\vartheta_c(x')} \rangle \sim |x - x'|^{-1/K_c}, \quad (9)$$

and the only parameter controlling contribution of the gapless charge degrees of freedom to the infrared properties of the system is the charge LL parameter K_c .

The infrared behavior of the Sine-Gordon Hamiltonian \mathcal{H}_s is described by the corresponding pair of renormalization group (RG) equations for the effective coupling constants $K_s(l)$ and $M_s(l)$

$$\begin{aligned} \frac{dM_s(L)}{dL} &= -2(K_s(L) - 1)M_s(L) \\ \frac{dK_s(L)}{dL} &= -\frac{1}{2}M_s^2(L) \end{aligned} \quad (10)$$

where $L = \ln(a_0)$, $K_s(L = 0) = 1 + \frac{1}{2}g_{0s}$ and $M_s(L = 0) = g_{\perp}/2\pi$. The pair of RG equations (10) describes the Kosterlitz-Thouless transition [33] in the spin channel. The flow lines lie on the hyperbola

$$4(K_s - 1)^2 - M_s^2 = \mu_{\pm}^2 = g_{0s}^2 - g_{\perp}^2 \quad (11)$$

and depending on the relation between the bare coupling constants g_{0s} and g_{\perp} exhibit two different regimes [34]:

Weak-coupling regime. For $g_{0s} \geq |g_{\perp}|$ we are in the weak-coupling regime with effective mass $\mathcal{M}_s \rightarrow 0$. The low energy (large distance) behavior of the corresponding gapless mode is described by a free scalar field.

The vacuum averages of exponentials of the corresponding fields show a power-law decay at large distances,

$$\langle e^{i\sqrt{2\pi}\varphi_s(x)} e^{-i\sqrt{2\pi}\varphi_s(x')} \rangle \sim |x - x'|^{-K_s^*}, \quad (12)$$

$$\langle e^{i\sqrt{2\pi}\vartheta_s(x)} e^{-i\sqrt{2\pi}\vartheta_s(x')} \rangle \sim |x - x'|^{-1/K_s^*}, \quad (13)$$

and the only parameter controlling the infrared behavior in the gapless regime is the fixed-point value of the effective coupling constants $K_s^* = K_s(l = \infty)$ determined from equation (11).

Strong coupling regime. For $2(K_s^0 - 1) < |M_s^0|$ the system scales to strong coupling: depending on the sign of the bare mass M_s^0 , the renormalized mass \mathcal{M}_s is driven to $\pm\infty$, signaling a crossover to one of two strong coupling regimes with a dynamical generation of a commensurability gap in the excitation spectrum. The flow of $|\mathcal{M}_s|$ to large values indicates that the $\mathcal{M}_s \cos\sqrt{8\pi}\varphi_s$ term in the sine-Gordon model dominates the long-distance properties of the system. Depending on the sign of the mass term, the field φ_s gets ordered with expectation values [35]

$$\langle \varphi_s \rangle = \begin{cases} \sqrt{\pi/8} & (M_s^0 > 0) \\ 0 & (M_s^0 < 0) \end{cases}. \quad (14)$$

It easy to check that, using the initial values of the coupling constants given in (6)–(7), we obtain the following condition for generation of a gap in the spin excitation spectrum

$$\left| U - J_{xy} - \frac{J_z}{2} \cos(2\pi\nu) \right| > U - J_{xy} \cos(2\pi\nu) - J_z + \frac{J_z}{2} \cos(2\pi\nu). \quad (15)$$

2.1 Order parameters

To clarify the symmetry properties of the ground states of the system in different sectors we consider the following set of order parameters corresponding to the smooth “*sm*” and staggered “*st*” parts of:

1) the on-site density operator

$$\rho(n) \Rightarrow \rho_{sm}(x) + \rho_{st}(x)$$

where

$$\rho_{sm}(x) \simeq \sqrt{\frac{2}{\pi}} \partial_x \varphi_c(x), \quad (16)$$

$$\rho_{st}(x) \equiv \mathcal{O}_{CDW}(x) \simeq \sin(\sqrt{2\pi}\varphi_c - 2k_F x) \cos(\sqrt{2\pi}\varphi_s), \quad (17)$$

2) the on-site spin-density

$$\mathbf{S}_n \Rightarrow \mathbf{S}_{sm}(x) + \mathbf{S}_{st}(x) \quad (18)$$

where

$$S_{sm}^z(n) \equiv \mathcal{O}_{FM}^z(x) \simeq \frac{1}{\sqrt{2\pi}} \partial_x \varphi_s(x), \quad (19)$$

$$S_{sm}^x(n) \equiv \mathcal{O}_{FM}^x(x) \simeq \sin(\sqrt{2\pi}\varphi_s) \cos(\sqrt{2\pi}\vartheta_s), \quad (20)$$

$$S_{sm}^y(n) \equiv \mathcal{O}_{FM}^y(x) \simeq \sin(\sqrt{2\pi}\varphi_s) \sin(\sqrt{2\pi}\vartheta_s), \quad (21)$$

and

$$S_{st}^z(n) \equiv \mathcal{O}_{SDW^z}(x) \simeq \cos(\sqrt{2\pi}\varphi_c + 2k_F x) \sin(\sqrt{2\pi}\varphi_s), \quad (22)$$

$$S_{st}^x(n) \equiv \mathcal{O}_{SDW^x}(x) \simeq \cos(\sqrt{2\pi}\varphi_c + 2k_F x) \sin(\sqrt{2\pi}\vartheta_s), \quad (23)$$

$$S_{st}^z(n) \equiv \mathcal{O}_{SDW^y}(x) \simeq \cos(\sqrt{2\pi}\varphi_c + 2k_F x) \cos(\sqrt{2\pi}\vartheta_s). \quad (24)$$

In addition we use the following set of superconducting order parameters:

3a) the on-site singlet

$$c_{n,\uparrow}^\dagger c_{n,\downarrow}^\dagger \Rightarrow \mathcal{O}_{SS}^\dagger(x) + \mathcal{O}_{\eta-SS}^\dagger(x) \quad (25)$$

3b) the extended singlet

$$\frac{1}{\sqrt{2}} \left(c_{n,\uparrow}^\dagger c_{n+1,\downarrow}^\dagger - c_{n,\downarrow}^\dagger c_{n+1,\uparrow}^\dagger \right) \Rightarrow \mathcal{O}_{ES}^\dagger(x) + \mathcal{O}_{\eta-ES}^\dagger(x) \quad (26)$$

3c) and the triplet pairing

$$\frac{1}{\sqrt{2}} \left(c_{n,\uparrow}^\dagger c_{n+1,\downarrow}^\dagger + c_{n,\downarrow}^\dagger c_{n+1,\uparrow}^\dagger \right) \Rightarrow \mathcal{O}_{TS^0}^\dagger(x) + \mathcal{O}_{\eta-TS^0}^\dagger(x) \quad (27)$$

$$\frac{1}{\sqrt{2}} \left(c_{n,\uparrow}^\dagger c_{n+1,\uparrow}^\dagger \pm c_{n,\downarrow}^\dagger c_{n+1,\downarrow}^\dagger \right) \Rightarrow \mathcal{O}_{TS^{xy}}^\dagger(x). \quad (28)$$

Here operators without and with the subscript η correspond, respectively, to the smooth and $2k_F$ -modulated (staggered) parts of the corresponding superconducting order parameters.

The bosonized expressions for the smooth parts of the corresponding superconducting order parameters, up to the accuracy of irrelevant ν -dependent amplitudes and phase shifts are given by

$$\mathcal{O}_{SS}^\dagger(x) \sim \mathcal{O}_{ES}^\dagger(x) \sim \cos(\sqrt{2\pi}\varphi_s) e^{i\sqrt{2\pi}\vartheta_c}, \quad (29)$$

$$\mathcal{O}_{TS^0}^\dagger(x) \sim \sin(\sqrt{2\pi}\varphi_s) e^{i\sqrt{2\pi}\vartheta_c}, \quad (30)$$

$$\mathcal{O}_{TS^{xy}}^\dagger(x) \sim \begin{cases} \cos(\sqrt{2\pi}\vartheta_s) e^{i\sqrt{2\pi}\vartheta_c} \\ \sin(\sqrt{2\pi}\vartheta_s) e^{i\sqrt{2\pi}\vartheta_c}. \end{cases} \quad (31)$$

Similarly the bosonized expression for the staggered components of the corresponding superconducting order parameters are given by

$$\begin{aligned} \mathcal{O}_{\eta-SS}^\dagger(x) &\sim \mathcal{O}_{\eta-ES}^\dagger(x) \sim \mathcal{O}_{\eta-TS^0}^\dagger(x) \\ &\sim \sin(\sqrt{2\pi}\varphi_c + 2k_F x) e^{i\sqrt{2\pi}\vartheta_c}, \end{aligned} \quad (32)$$

Note that the smooth part in equation (25) corresponds to the usual BCS-type pairing while at half-filling the oscillating terms in (25) and (26) describe the weak-coupling analogs of the η -pairing superconductivity [36].

3 The weak-coupling phase diagram

In this section we consider the ground state phase diagram of the model (1) away from the commensurate value of the 1/2-filled band. Due to the invariance of the model parameters under the transformation $\nu \rightarrow 1 - \nu$ we restrict our consideration to the sector $0 < \nu < 1/2$. Below we consider the the weak-coupling ground state phase at quarter-filling in detail, while for $\nu \neq 1/4$ we present a qualitative description of the phase diagram.

3.1 The $U = 0$ case

Let us start with the case $U = 0$ where the basic equations read:

$$K_c \simeq 1 + \frac{1}{2\pi v_F} \left(J_{xy} + \frac{1}{2} J_z \right) \cos(2\pi\nu), \quad (33)$$

and

$$2(K_s - 1) \simeq -\frac{1}{\pi v_F} \left[J_z + (J_{xy} - \frac{1}{2} J_z) \cos(2\pi\nu) \right], \quad (34)$$

$$2\pi m_s \simeq -\frac{1}{\pi v_F} \left[J_{xy} + \frac{1}{2} J_z \cos(2\pi\nu) \right]. \quad (35)$$

In the following we study the two cases $\nu = 1/4$ and $\nu \neq 1/4$ separately.

3.1.1 $\nu = 1/4$

At $U = 0$ the charge sector is featureless with $K_c = 1$ independently from the values of the exchange couplings J_z and J_{xy} . Since the charge sector is featureless, the ground

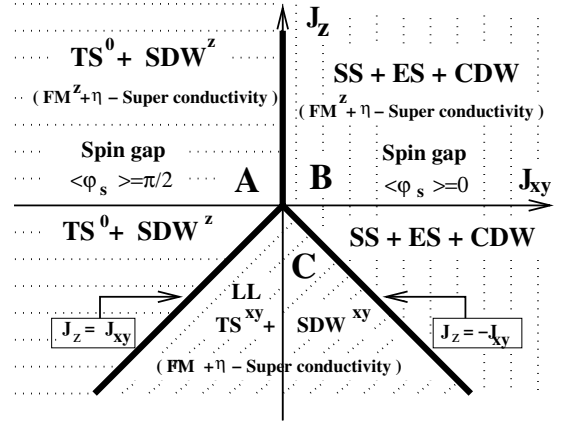


Fig. 1. The ground state phase diagram of the 1/4-filled itinerant $t - J_{xy} - J_z$ model. The thick solid lines indicate borders between the weak-coupling limit phases. Along these lines and in the sector C the spin excitations are gapless. The charge excitation spectrum is gapless in all sectors of the phase diagram.

state phase diagram is completely determined only by the spin degrees of freedom. The condition for dynamical generation of a spin gap reads $|-J_{xy}| > -J_z$ and thus the spin sector is gapless for $J_z \leq -|J_{xy}|$ and along the semi-axis $J_z \geq 0$. These conditions determine the following three sectors of the phase diagram (see Fig. 1):

The sector **A** ($J_{xy} < 0, J_z > -J_{xy}$) corresponds to a spin gapped phase with dominating SDW^z and TS^0 ordering. These correlations decay as power-laws at large distances:

$$\langle \mathcal{O}_{SDW^z}(0) \mathcal{O}_{SDW^z}(r) \rangle \simeq \cos(\pi r/2) \cdot r^{-1}, \quad (36)$$

$$\langle \mathcal{O}_{TS^0}(0) \mathcal{O}_{TS^0}(r) \rangle \simeq r^{-1}. \quad (37)$$

The longitudinal ferromagnetic and the η -superconducting correlations decay faster as

$$\langle \mathcal{O}_{FM^z}(0) \mathcal{O}_{FM^z}(r) \rangle \simeq r^{-2}, \quad (38)$$

$$\begin{aligned} \langle \mathcal{O}_{\eta-SS}(0) \mathcal{O}_{\eta-SS}(r) \rangle &\simeq \langle \mathcal{O}_{\eta-ES}(0) \mathcal{O}_{\eta-ES}(r) \rangle \\ &\simeq \langle \mathcal{O}_{\eta-TS^0}(0) \mathcal{O}_{\eta-TS^0}(r) \rangle \simeq \cos(\pi r/2) \cdot r^{-2}. \end{aligned} \quad (39)$$

Other correlations decay exponentially.

The sector **B** ($J_{xy} > 0, J_z > -J_{xy}$) corresponds to a spin gapped phase with dominating SS, ES and CDW ordering. The corresponding correlations show a power-law decay at large distances:

$$\langle \mathcal{O}_{SS}(0) \mathcal{O}_{SS}(r) \rangle = \langle \mathcal{O}_{ES}(0) \mathcal{O}_{ES}(r) \rangle \simeq r^{-1}, \quad (40)$$

$$\langle \mathcal{O}_{CDW}(0) \mathcal{O}_{CDW}(r) \rangle \simeq \cos(\pi r/2) \cdot r^{-1}. \quad (41)$$

In this case also the longitudinal ferromagnetic and the η -superconducting correlations decay faster (38) and (39), while all other correlations are exponentially suppressed.

In the sector **C** ($J_z < -|J_{xy}|$) the gapless Luttinger Liquid (LL) phase is realized. All correlations decay as power-laws, however the transverse antiferromagnetic and triplet superconducting instabilities are the dominating

instabilities in this sector. The corresponding correlations decay as

$$\langle \mathcal{O}_{SDW^{xy}}(0) \mathcal{O}_{SDW^{xy}}(r) \rangle \simeq \cos(\pi r/2) r^{-1-1/K_s^*}, \quad (42)$$

$$\langle \mathcal{O}_{TS^{xy}}(0) \mathcal{O}_{TS^{xy}}(r) \rangle \simeq r^{-1-1/K_s^*}, \quad (43)$$

where the fixed point value of the spin LL parameter

$$K_s^* = 1 + \frac{1}{2\pi v_F} \sqrt{J_z^2 - J_{xy}^2} > 1. \quad (44)$$

Since the spin stiffness parameter $K_s^* > 1$, the longitudinal ferromagnetic and the η -superconducting correlations given by equations (37) and (38) decay faster and are the subleading instabilities in this sector. The transverse ferromagnetic correlations decay even faster as

$$\langle \mathcal{O}_{FM^{x,y}}(0) \mathcal{O}_{FM^{x,y}}(r) \rangle \simeq r^{-K_s^*-1/K_s^*}. \quad (45)$$

However, within the accuracy of the used first order RG approach their decay is the same as of the longitudinal ferromagnetic correlations (38).

Finally, the CDW , SDW^z and the TS^0 correlations decay as

$$\langle \mathcal{O}_{CDW}(0) \mathcal{O}_{CDW}(r) \rangle \simeq \langle \mathcal{O}_{SDW}^z(0) \mathcal{O}_{SDW}^z(r) \rangle \simeq \cos(\pi r/2) \cdot r^{-1-K_s^*}, \quad (46)$$

$$\langle \mathcal{O}_{TS^0}(0) \mathcal{O}_{TS^0}(r) \rangle \simeq r^{-1-K_s^*}, \quad (47)$$

and correspond to the weakest instabilities in this sector.

3.1.2 $\nu \neq 1/4$

At $\nu \neq 1/4$ the charge stiffness parameter $K_c \neq 1$ and therefore the line $J_z = -2J_{xy}$ divides the parameter space into two semiplanes: the part with dominating CDW or SDW instabilities at $K_c < 1$ and the part with dominating superconducting instabilities at $K_c > 1$. However, the effect of charge sector essentially depends on the band-filling.

At $1/4 < \nu < 1/2$, $K_c - 1 \sim \text{sign}(J_z + 2J_{xy})$. Therefore the dynamical generation of a spin gap and subsequent pinning of the spin field with vacuum expectation value $\langle \varphi_s \rangle = \pi/2$ results to metallic phase with dominating Triplet Superconducting (TS^0) instability at $J_{xy} < 0$, $J_{xy} < J_z < -2J_{xy}$ and dominating antiferromagnetic SDW^z at $-0.5J_z < J_{xy} < -0.5 \cos(2\pi\nu)J_z$ (see Fig. 2, sectors A and B respectively).

In the sector C of the phase diagram, at $-2J_{xy} \cos^2(\pi\nu) < J_z < -2J_{xy}/\cos(2\pi\nu)$, the spin gapped metallic phase with dominating CDW phase is realized.

In the Luttinger Liquid sectors of the phase diagram D and E, at $J_z < \min\{J_{xy}, -2 \cos^2(\pi\nu)J_{xy}\}$ the line $J_z = -2J_{xy}$ marks the transition from a LL phase with dominating TS^{xy} instability at $J_z < \min\{J_{xy}, -2J_{xy}\}$ (see Fig. 2, sector E) to a LL phase with dominating transverse antiferromagnetic instabilities SDW^{xy} at $-2J_{xy} < J_z < -2 \cos^2(\pi\nu)J_{xy}$ (see Fig. 2, sector D). One has to note,

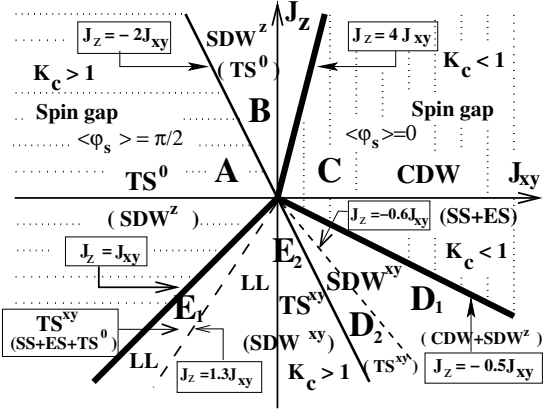


Fig. 2. The ground state phase diagram of the 1/3-filled itinerant $t - J_{xy} - J_z$ model. The thick solid lines denote lines in the parameter space where the spin gap opens and indicate borders between the weak-coupling limit phases. The thin solid line corresponds to the line $K_c = 1$ and marks the transition from the sector of phase diagram with dominating density instabilities ($K_c < 1$) into the sector with dominating superconducting ordering ($K_c > 1$). The dashed lines mark (qualitatively) the crossover areas between the Luttinger Liquid phases with different sets of subleading instabilities. The phases A and B, as well as the D_2 and E_2 phases are characterized by an identical excitation spectrum and interchange of leading and subleading instabilities. The subleading instabilities are indicated in brackets.

that for a given band-width $\nu \neq 1/4$ in the LL sectors D and E, there are additional “subdominant order crossover” lines (marked by dashed lines in Figs. 2 and 3) which separate two areas with two different subdominant order. In particular, in the subsector E_1 the subdominant order is $SS + ES + TS^0$ and in the subsector E_2 it is SDW^{xy} . Similarly, in the subsector D_1 the subdominant order is $CDW + SDW^z$ and in the subsector D_2 it is TS^{xy} .

On the other hand, at $\nu < 1/4$ (see Fig. 3) the A sector corresponds to the spin gapped metallic state with dominating SDW^z instabilities, while triplet superconductivity TS^0 is the dominating instability in the narrow stripe of sector B. Similarly, in the sector C at $J_z > \max\{-2J_{xy}/\cos(2\pi\nu), -2J_{xy} \cos^2(\pi\nu)\}$ a spin gapped phase with dominating tendencies towards singlet superconducting ordering is realized. Similarly in the Luttinger liquid phase dominant and subdominant instabilities in the sectors D and E change places, i.e. in sector D the dominant order is TS^{xy} and the subdominant order in sector D_1 is $SS + ES + TS^0$ and in sector D_2 it is SDW^{xy} . In sector E the dominant order is SDW^{xy} and the subdominant order in sector E_1 is $SDW^z + CDW$ and in sector E_2 it is TS^{xy} .

3.2 The $J_z = 0$ case

At $J_z = 0$ the basic equations read:

$$K_c \simeq 1 - \frac{1}{2\pi v_F} (U - J_{xy} \cos(2\pi\nu)), \quad (48)$$

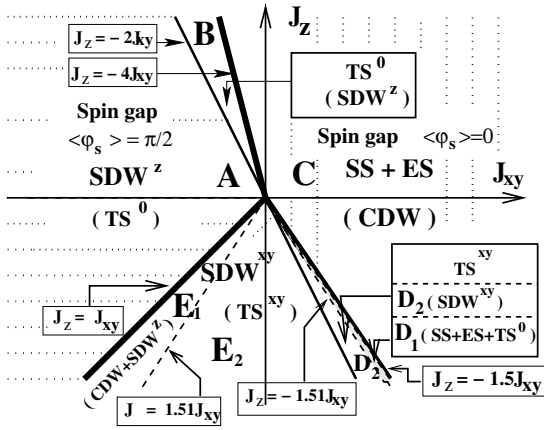


Fig. 3. The ground state phase diagram of the $1/6$ -filled itinerant $t - J_{xy} - J_z$ model. Solid lines indicate borders between the weak-coupling limit phases. The thick solid lines denote lines in the parameter space where the spin gap opens and indicate borders between the weak-coupling limit phases. The thin solid line $J_z = -2J_{xy}$ marks the transition from the sector of phase diagram with dominating density instabilities ($K_c < 1$) into the sector with dominated superconducting ordering ($K_c > 1$). The dashed lines mark (qualitatively) the crossover areas between the Luttinger Liquid phases with different sets of subleading instabilities. The phases A and B, as well as the D_2 and E_2 phases are characterized by an identical excitation spectrum and interchange of leading and subleading instabilities. The subleading instabilities are indicated in brackets.

and

$$2(K_s - 1) \simeq \frac{1}{\pi v_F} \left[U - J_{xy} \cos(2\pi\nu) \right], \quad (49)$$

$$2\pi m_s \simeq \frac{1}{\pi v_F} \left[U - J_{xy} \right]. \quad (50)$$

Again we distinguish the cases $\nu = 1/4$ and $\nu \neq 1/4$ in the following.

3.2.1 $\nu = 1/4$

At $U \neq 0$, even for $\nu = 1/4$ the charge stiffness parameter $K_c \neq 1$ and therefore the line $U = 0$ divides the parameter space into two parts, the part with dominating CDW or SDW instabilities at $U > 0$ ($K_c < 1$) and the part with dominating superconducting instabilities at $U < 0$ i.e. ($K_c > 1$).

At $J_{xy} < 0$ and $U > J_{xy}$ the spin sector is gapped and the spin field gets ordered with vacuum expectation value $\langle \varphi_s \rangle = \pi/2$. This leads to the suppression of all instabilities whose power-law decay is less than $1/r^2$ except the SDW^z and TS^0 ones, which show a power-law decay

$$\langle \mathcal{O}_{SDW^z}(0) \mathcal{O}_{SDW^z}(r) \rangle \simeq r^{-K_c} \cos(2\pi\nu r) \quad (51)$$

$$\langle \mathcal{O}_{TS^0}(0) \mathcal{O}_{TS^0}(r) \rangle \simeq r^{-1/K_c}. \quad (52)$$

Therefore, in the sector **A**, at $J_{xy} < 0 < U$ the SDW^z is the dominating instability in the system and in the sector **E** at $J_{xy} < U < 0$ the triplet superconducting ordering dominates.

For $U < J_{xy} < 0$ and for $U < J_{xy}/2$ the spin sector is also gapped but the vacuum expectation value of the ordered spin field $\langle \varphi_s \rangle = 0$. This leads to suppression of all instabilities with power-law decay less than $1/r^2$ except density-density and singlet superconducting instabilities, which show the following power-law decay

$$\langle \mathcal{O}_{CDW}(0) \mathcal{O}_{CDW}(r) \rangle \simeq r^{-K_c} \cos(2\pi\nu r) \quad (53)$$

$$\langle \mathcal{O}_{SS}(0) \mathcal{O}_{SS}(r) \rangle \simeq \langle \mathcal{O}_{ES}(0) \mathcal{O}_{ES}(r) \rangle \simeq r^{-1/K_c}. \quad (54)$$

Therefore in the sector **C** at $0 < U < J_{xy}/2$ the CDW ordering dominates, while in the sector **D** at $U < \min\{0, J_{xy}\}$ the singlet superconducting order is realized.

Finally, in the sector **B** ($U > J_{xy}/2$) the LL phase with gapless charge and spin excitation spectrum and dominating easy-plane antiferromagnetic ordering is realized in the ground state. The corresponding correlations show a power-law decay

$$\langle \mathcal{O}_{SDW^{xy}}(0) \mathcal{O}_{SDW^{xy}}(r) \rangle \simeq r^{-K_c - 1/K_s^*}, \quad (55)$$

where the fixed point value of the spin stiffness parameter is given by

$$K_s^* = 1 + \frac{1}{2\pi v_F} \sqrt{J_{xy}(2U - J_{xy})}. \quad (56)$$

One can easily show that the CDW and SDW^z correlations decay faster

$$\begin{aligned} \langle \mathcal{O}_{CDW}(0) \mathcal{O}_{CDW}(r) \rangle &\simeq \\ \langle \mathcal{O}_{SDW^z}(0) \mathcal{O}_{SDW^z}(r) \rangle &\simeq r^{-K_c - K_s^*}, \end{aligned} \quad (57)$$

and are the subleading instabilities in this sector.

3.2.2 $\nu \neq 1/4$

At $\nu \neq 1/4$ the phase diagram is qualitatively the same as at quarter-filling (see Fig. 4). The minor difference consist of the ν dependence of the border lines which mark transitions between different phases. In particular:

- 1) the semiplane in the parameter space corresponding to dominant density-density correlations (sectors A, B and C in the phase diagram) is separated from the semiplane with dominant superconducting ordering (sectors E and D) by the line $U = J_{xy} \cos(2\pi\nu)$;
- 2) the line $U = J_{xy} \cos^2(\pi\nu)$ corresponds to the border line between the B and C sectors of the phase diagram.

To conclude this section, we have shown that the weak-coupling phase diagram of the non-half-filled itinerant $t - J - U$ model shows a triplet superconducting ordering in the sector of the phase diagram with dominating ferromagnetic exchange and easy-plane anisotropy. However, as it was shown in reference [31] in the case of half-filled

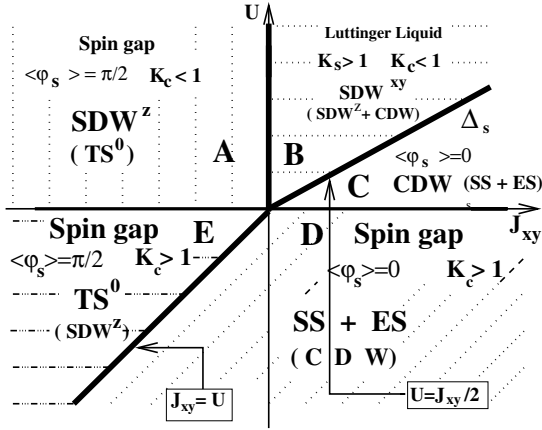


Fig. 4. The ground state phase diagram of the 1/4-filled itinerant $t - J_{xy} - U$ model. Solid lines indicate borders between the weak-coupling limit phases. The thick solid lines denote lines in the parameter space where the spin gap opens and indicate borders between the weak-coupling limit phases. The thin solid line $U = 0$ marks the transition from the sector of phase diagram with dominating density instabilities ($K_c < 1$) into the sector with dominated superconducting ordering ($K_c > 1$). The subleading instabilities are indicated in brackets.

band and for transverse ferromagnetic exchange stronger than some critical value $J_{xy} < J_{xy}^c$ ($-J_{xy}^c \simeq W$, where W is the bandwidth), the transition into an insulating phase with easy-plane type ferromagnetic ordering takes place.

Although the transition into the gapless phase with ferromagnetic order (ferrometal) at $\nu \neq 1/2$ is a pure finite-bandwidth, strong coupling effect, the very presence of this transition as well as a clear asymmetry between antiferromagnetic ($J_{xy} > 0$) and ferromagnetic ($J_{xy} < 0$) exchange can be traced already within the weak-coupling treatment, if we take into account the Hartree regularization of the hopping amplitude given by $t_{\text{eff}} = t(1 + \gamma J_{xy}/2\pi t)$. Here $\gamma(\nu) > 0$ is a band-filling dependent parameter, which is of the order of unity for the band-fillings considered in this paper. It is clear that in the case of antiferromagnetic transverse exchange the effective bandwidth increases, while for ferromagnetic coupling it reduces. The weak-coupling approach fails when the effective dimensionless coupling constant $|g_i| = |J_{xy}|/\pi v_F$ becomes of the order of unity. Taking into account the Hartree renormalization of the Fermi velocity we estimate the range of applicability of the weak-coupling approach as $|J_{xy}| < \pi t$. In this sector of the parameter space with strong easy-plane anisotropy $|g_{\perp}| > |g_{0s}|$ the soliton mass of the sine-Gordon field (3) is given by $M_s \simeq W \exp(-\pi W/2|J_{xy}|)$ [32] and therefore for $|J_{xy}| \leq \pi t$ the spin gap increases with increasing strength of the transverse ferromagnetic exchange. However, since in the case of strong ferromagnetic exchange $J_{xy} \leq -\pi t$ the effective bandwidth $W \sim t_{\text{eff}}$ tends to zero, the initial increase of the spin gap should change into a decrease caused by the collapse of the bandwidth W . As we show below, using the DMRG studies of chains up to $L = 120$ sites, this is indeed the case. For $J_{xy} < 0$, the spin gap as a function of the pa-

rameter J_{xy} shows a bellshaped behavior with maximum at $J_{xy} \simeq -\pi t$ and reaches zero at $J_{xy} = J_{xy}^{(c1)} \simeq -4t$. At $J < J_{xy}^{(c1)}$ the ground state of the system is similar to that of the $t - J_{xy}$ model with gapless charge (due to the doping) and gapless spin (due to the in-plane, XY character of the exchange) excitation spectrum.

4 Numerical results for $J_z = 0$ and $\nu = 1/4$

In order to check the validity of the picture suggested by the bosonization results derived in the previous sections we use the density-matrix renormalization-group (DMRG) method [37–39]. As in our previous study [31] it is applied to open chains up to 120 sites keeping typically 400 states in each block using the *infinite-size* algorithm to determine the ground-state properties, including correlation functions.

Below we focus on the case of a quarter-filled band and $J_z = 0$.

4.1 Excitation spectrum

First we determine the low-lying spin and charge excitations as function of the transverse spin exchange J_{xy} . In the numerical calculations, we have found that for open boundary conditions the ground state energy for a system of L sites with N_{\uparrow} up-spin and N_{\downarrow} down-spin electrons $E_0^{(L)}(N_{\uparrow}, N_{\downarrow})$ remains in the sector with the “z” component of the total spin $S_{\text{tot}}^z = 0$ (i.e. $N_{\uparrow} = N_{\downarrow} = N/2$, where $N = N_{\uparrow} + N_{\downarrow}$ is the total number of electrons) for all parameter values studied here.

As it is commonly used in literature, gaps to excitations classified as *charge excitations* are calculated by taking the difference between ground-state energies with different number of particles. It is convenient to stay in the sector with $S_{\text{tot}}^z = 0$ and therefore the charge gap is evaluated by

$$\Delta_c(L) = \frac{1}{2} \left[E_0^{(L)} \left(\frac{N}{2} + 1, \frac{N}{2} + 1 \right) + E_0^{(L)} \left(\frac{N}{2} - 1, \frac{N}{2} - 1 \right) - 2E_0^{(L)} \left(\frac{N}{2}, \frac{N}{2} \right) \right]. \quad (58)$$

We determine the spin gap as the difference between the lowest energy in the sector with $S_{\text{tot}}^z = 0$ ($N_{\uparrow} - N_{\downarrow} = 2$) and the ground state energy

$$\Delta_s(L) = E_0^{(L)} \left(\frac{N}{2} + 1, \frac{N}{2} - 1 \right) - E_0^{(L)} \left(\frac{N}{2}, \frac{N}{2} \right). \quad (59)$$

The results for finite chains are extrapolated for $L \rightarrow \infty$ by fitting a polynomial in $1/L$. As expected the charge gap $\Delta_c = \lim_{L \rightarrow \infty} \Delta_c(L)$ vanishes for all values of J_{xy} . On the other hand, the spin gap $\Delta_s = \lim_{L \rightarrow \infty} \Delta_s(L)$ shows a nontrivial behavior where five different regimes can be distinguished (Fig. 5).

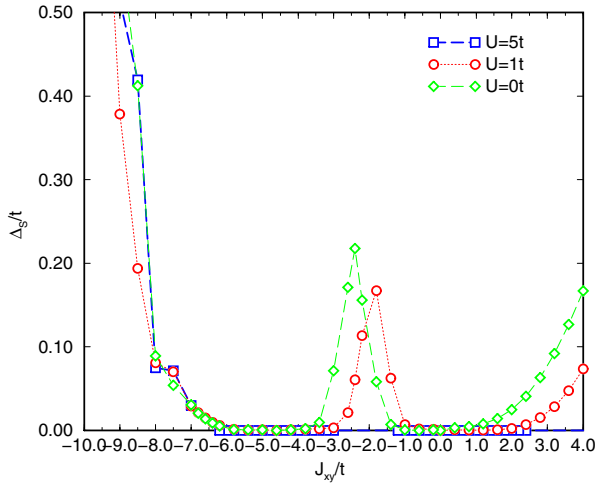


Fig. 5. Spin gap Δ_s of the itinerant XY model at quarter filling, $t = 1$, $J_z = 0$ and $U = 0$ (diamonds), $U = 1$ (circles) and $U = 5$ (squares). The charge gap Δ_c vanishes for all J_{xy} .

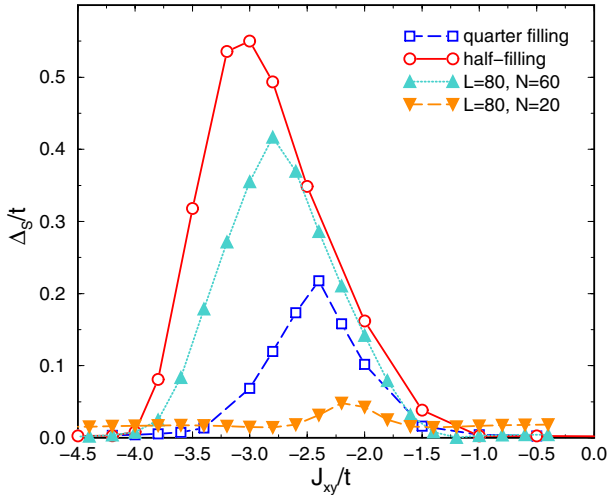


Fig. 6. Spin gap Δ_s of the itinerant ferromagnetic XY model ($J_{xy} < 0$) at $U = 0$ and for fillings $\nu = 1/2, 1/4, 3/8, 1/8$.

In agreement with predictions of the weak-coupling treatment, at $U = 0$ and weak exchange $|J_{xy}|$ the spin sector is gapped for both signs of the transverse exchange. With increasing antiferromagnetic exchange the spectrum remains gapped, while in the case of ferromagnetic exchange, at $J_{xy} \simeq -2.5t$ the spin gap starts to decrease and becomes zero at $J_{xy}^c \simeq -3.4t$. The spin gapless phase remains till $J_{xy}^c \simeq -5.8t$ where the spin gap opens once again.

Thus three gapful regimes (for large ferro- and antiferromagnetic couplings and for intermediate ferromagnetic exchange) are separated by two gapless regimes. As it is seen from Figure 5 a repulsive Coulomb interaction $U > 0$ only changes this behaviour quantitatively. The gap is slightly suppressed and the gapful regimes appear at larger values of the exchange interaction J_{xy} .

We have also checked the band-filling dependence of the spin-gapped phase for intermediate ferromagnetic ex-

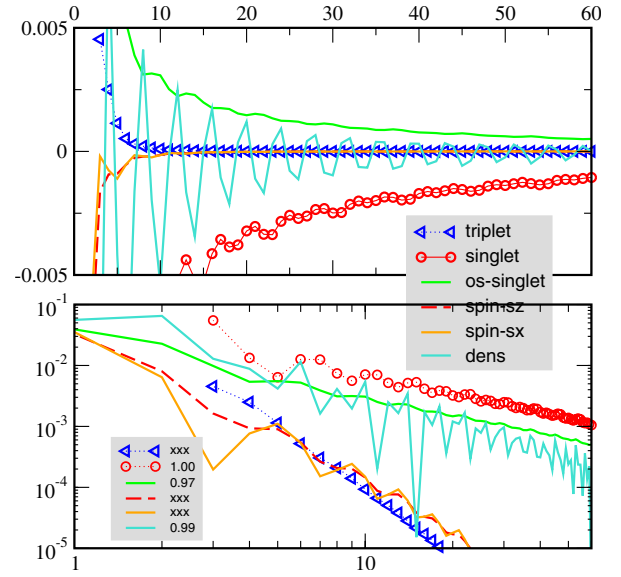


Fig. 7. Correlation functions, plotted against the real space distance $|i-j|$, in the case of strong antiferromagnetic exchange $J_{xy} = 3.8t$ and $U = 0$. The lower figure shows the decay of the correlations, plotted on a double logarithmic scale. Numbers in the inset of the lower figure are the exponents. The notation “xxx” corresponds to the case of exponentially decaying correlations.

change. As it follows from Figure 6 the dome-type dependence of the spin gap on the increasing ferromagnetic transverse interaction qualitative remains unchanged at $\nu \neq 1/2$. Although position and value of the maximum of the spin gap depends on the band filling (Fig. 6) the effect of the closing of the spin gap at large ferromagnetic exchange is band-filling independent.

4.2 Correlation functions at $U = 0$

To investigate the nature of ordering in the different phases we study the behavior of the correlation functions. In the sectors with gapless excitation spectrum we expect the usual expression for correlation functions

$$C(r) \equiv \langle \mathcal{O}^\dagger(r) \mathcal{O}(0) \rangle \sim A_1 r^{-\theta_1} + \cos(2k_F r) A_2 r^{-\theta_2} \quad (60)$$

consisting of a smooth part decaying with exponent θ_1 and an oscillating part decaying with θ_2 . In determining the asymptotics of correlation functions we focus on the dominating part given by $\theta = \min\{\theta_1, \theta_2\}$.

In the following we will present results for correlation functions in different sectors of the phase diagram.

4.2.1 Sector I: $J_{xy} > 0$. The SS + ES + CDW phase

We start our consideration from the case antiferromagnetic exchange. In Figure 7 we have plotted results of DMRG calculations for correlation functions at $J_{xy} = 3.8t$ and $U = 0$.

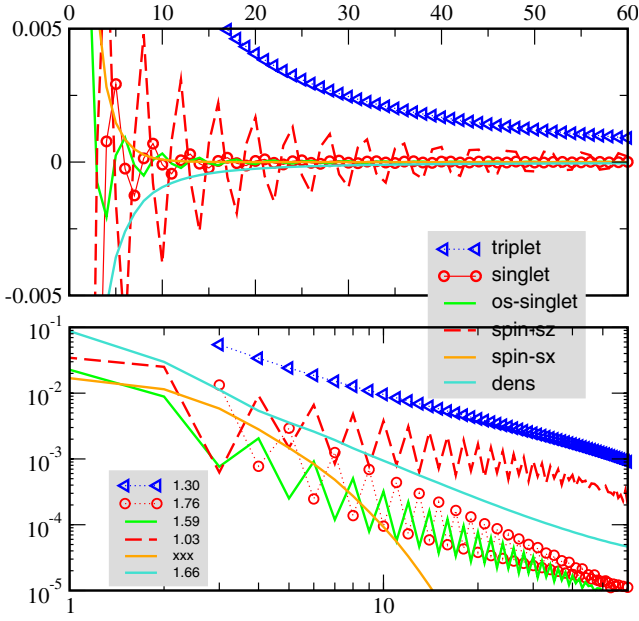


Fig. 8. Correlation functions, plotted against the real space distance $|i-j|$ in the case of ferromagnetic exchange $J_{xy} = -2.8t$ and $U = 0$. The lower figure shows the decay of the correlations, plotted on a double logarithmic scale. Numbers in the inset of the lower figure are the exponents. The notation “xxx” corresponds to the case of exponentially decaying correlations.

As it is clearly seen from Figure 7, in an excellent agreement with the bosonization results, the triplet superconducting and antiferromagnetic correlations are completely suppressed in this case, while the singlet superconducting and density-density correlations show an identical power-law decay with critical indices equal to one. The very small deviation of the numerically evaluated values of the exponents $\theta_{ES} = 0.97$ and $\theta_{CDW} = 0.98$ from the analytically predicted value $\theta_{SS} = \theta_{ES} = \theta_{CDW} = 1$ reflects the high accuracy of the obtained numerical results in this sector of the phase diagram.

4.2.2 Sector II: $J_{xy}^c < J_{xy} < 0$. The $SDW^z + TS^0$ phase

Let us now consider the case of ferromagnetic exchange. At $J_{xy} < 0$ and $U = 0$, the weak-coupling bosonization results predict exponential suppression of the CDW and singlet correlations, whereas SDW^z and triplet correlators TS^0 show a power-law decay (cf. with Eqs. (36), (37)). Furthermore, they are the dominating instabilities in this phase.

Figure 8 displays DMRG results for the correlation functions. One can clearly observe a strong SDW^z and TS^0 correlation in the ground state. In addition, from the double logarithmic plot one obtains that the in-plane magnetic correlations decay exponentially, while the density and singlet-superconducting correlations show an almost identical power-law decay at large distances. This is expected from the bosonization results, since, due to the

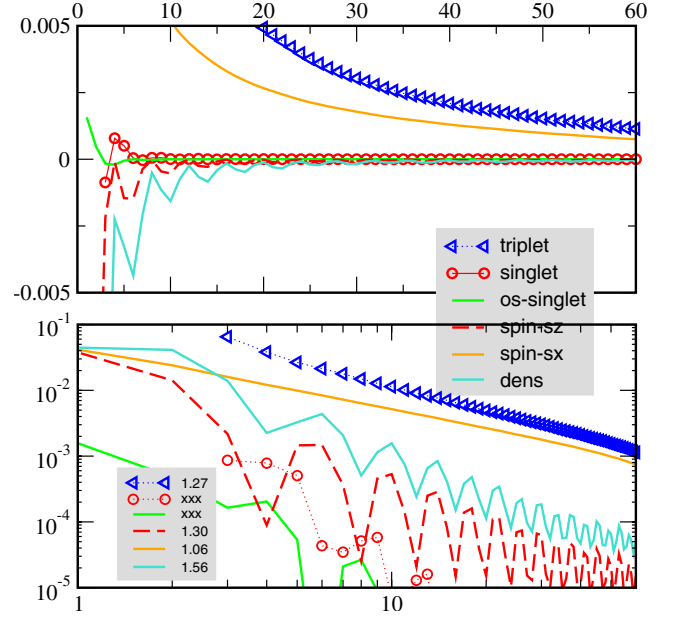


Fig. 9. Correlation functions, plotted against the real space distance $|i-j|$, in the case of strong antiferromagnetic exchange $J_{xy} = -5.0t$ and $U = 0$. The lower figure shows decay of the correlations, plotted on a double logarithmic scale. Numbers in the inset of the lower figure are the exponents. The notation “xxx” corresponds to the case of exponentially decaying correlations.

pinning of the spin Bose field with vacuum expectation value $\langle \sqrt{2\pi} K_s \varphi_s \rangle = \pi/2$, the in-plane magnetic correlations which are determined by the dual-field decay exponentially. The same reason of spin-field pinning leads to suppression of the oscillating part in the density correlations (clearly seen in Fig. 8) and to the suppression of the smooth part of the on-site singlet correlations. The latter is the reason why the on-site and extended singlet-pair correlations show an identical behavior.

4.2.3 Sector III: $J_{xy}^c < J_{xy} < J_{xy}^c$. The ferrometallic phase

In Figure 9 we have shown results of DMRG calculations for correlation functions for strong ferromagnetic coupling $J_{xy} = -5.0t$. In this sector, charge and spin gap vanish and the system shows properties of a metal with gapless spin degrees of freedom. As it is clearly seen, the transverse ferromagnetic and triplet superconducting instabilities dominate in the ground state. The lower figure in Figure 9 displays correlation functions plotted in a double logarithmic scale. As it follows from this figure, despite the gapless character of spin excitations, the singlet superconducting correlations are suppressed exponentially. At the same time, the SDW^z and CDW correlations also show power-law behavior, but decay slightly faster than the in-plane spin correlations. Clearly in this sector the system shows very unconventional behaviour, not consistent with the standard weak-coupling results.

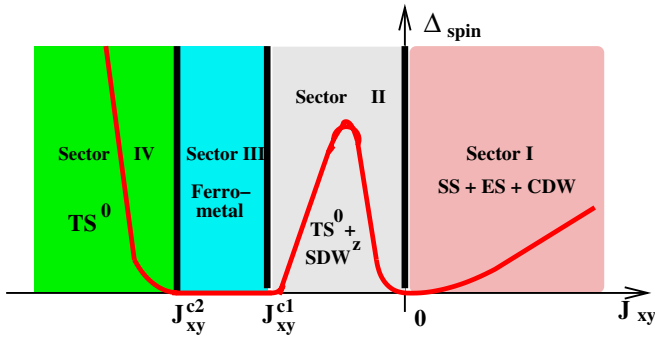


Fig. 10. Qualitative form of the ground state phase diagram for the $t - J_{XY} - U$ model at quarter-filling and $t = 1$ and $U > 0$. The bold red line shows the spin gap as a function of the parameter J_{xy} .

4.2.4 Sector IV: $J_{xy} < J_{xy}^{c2}$. The triplet superconducting phase

This is the most intriguing sector of the phase diagram. The spin excitation spectrum is gapped. Moreover, as it is clearly seen from Figure 5, the opening of the spin gap at $J_{xy} < J_{xy}^{c2} \simeq -5.8t$ is *independent* of the on-site repulsion U . This indicates that in this sector of the phase diagram the itinerant nature of the electron system is completely lost and the phase diagram is completely determined by the properties of the effective ferromagnetic $t - J_{xy}$ model. We expect that this sector of the phase diagram corresponds to a triplet superconducting phase.

5 Conclusions

Motivated by recent experimental findings that show evidence for the competition or even coexistence of superconductivity and magnetism we have continued our studies of the ground state properties of an itinerant XY model. Using a composite approach based on weak-coupling bosonization and DMRG studies for chains up to $L = 120$ sites we have studied the ground state phase diagram of the itinerant XY model away from half-filling.

Depending on the model parameters J_{xy} , $U \geq 0$ and the band-filling ν we have found evidence for five different phases in the ground state. Figure 10 summarizes our findings for the particular case of a quarter-filled band. Within the considered range of parameters the charge gap is always zero. The behavior of the spin gap as function of the spin-coupling J_{xy} allows to distinguish the following different phases:

1. For antiferromagnetic interactions $J_{xy} > 0$ the spin gapful metallic phase with dominating singlet superconducting and density-density correlations.
2. Approaching the line $J_{xy} = 0$ the spin gap closes and at this point the system shows properties of a Luttinger metal.
3. In the ferromagnetic sector at $-3.8t = J_{xy}^{c1} < J_{xy} < 0$ the spin gap is finite. It opens for arbitrary weak ferromagnetic XY -exchange, shows a dome-type shape

and closes at $J_{xy} = J_{xy}^{c1}$. In this sector of the phase diagram the system displays properties of a spin gapped metal with coexistence of triplet superconducting and spin-density-wave (SDW^z) instabilities.

4. At $-5.8t = J_{xy}^{c2} < J_{xy} < J_{xy}^{c1}$ a ferrometallic phase with gapless spin excitations and strongly dominating triplet superconducting and transverse ferromagnetic instabilities is realized in the ground state.
5. At $J_{xy} < J_{xy}^{c2}$ the spin gap opens once again. We expect that in this phase the system shows properties of a triplet superconductor. We have to stress that the effective ferromagnetic $t - J_{xy}$ model, which governs the behaviour of the system in this sector of the phase diagram, requires very detailed separate studies.

Although the presented numerical results are restricted to the case of quarter-filled band, our analysis indicates that qualitatively the phase diagram remains similar at $\nu \neq 1/4$. However, deviations from the commensurate value of the quarter-filled band remove the degeneracy in favour of density-density type ordering at $J_{xy} \cos(2\pi\nu) < 0$ and superconducting type ordering at $J_{xy} \cos(2\pi\nu) > 0$.

One of the interesting perspective for future studies would be the investigation of a genuine ferromagnetic $t - J$ -type model which should help to understand the limit of strong Coulomb repulsion better.

This work has been performed within the research program of the SFB 608 funded by the DFG. We thank Erwin Müller-Hartmann, Achim Rosch, Didier Poilblanc and Matthias Vojta for interesting discussions. IT also acknowledges support from the DAAD scholarship programs.

References

1. E. Dagotto, *Science* **309**, 257 (2005)
2. A.V. Chubukov, D. Pines, J. Schmalian, in *The Physics of Superconductors*, edited by K.H. Bennemann, J.B. Ketterson (Springer-Verlag, 2003), p. 495
3. D. Manske, *Theory of Unconventional Superconductors* (Springer, Heidelberg, 2004)
4. For a review, see A.P. Mackenzie, Y. Maeno, *Rev. Mod. Phys.* **75**, 657 (2003)
5. S.S. Saxena, P. Agarwal, K. Ahilan, F.M. Grosche, R.K.W. Haselwimmer, M.J. Steiner, E. Pugh, I.R. Walker, S.R. Julian, P. Monthoux, G.G. Lonzarich, A. Huxley, I. Sheikin, D. Braithwaite, J. Flouquet, *Nature* **406**, 587 (2000)
6. D. Aoki, A. Huxley, E. Ressouche, D. Braithwaite, J. Flouquet, J-P. Brison, E. Lhotel, C. Paulsen, *Nature* **413**, 613 (2001)
7. C. Pfleiderer, M. Uhlarz, S.M. Hayden, R. Vollmer, H.V. Löhneysen, N.R. Bernhoeft, G.G. Lonzarich, *Nature* **412**, 58 (2001)
8. T.M. Rice, M. Sigrist, *J. Phys.: Condens. Matter* **7**, L643 (1995)
9. I.I. Mazin, D.J. Singh, *Phys. Rev. Lett.* **79**, 733 (1997)
10. M. Sigrist, D. Agterberg, A. Furusaki, C. Honerkamp, K.K. Ng, T.M. Rice, M.E. Zhitomirsky, *Physica C* **317–318**, 134 (1999)
11. T.R. Kirkpatrick, D. Belitz, T. Vojta, R. Narayanan, *Phys. Rev. Lett.* **87**, 127003 (2001)

12. D.J. Singh, I.I. Mazin, Phys. Rev. Lett. **88**, 187004 (2002)
13. M.B. Walker, K.V. Samokhin, Phys. Rev. Lett. **88**, 227001 (2002)
14. A.V. Chubukov, A.M. Finkel'stein, R. Haslinger, D.K. Morr, Phys. Rev. Lett. **90**, 077002 (2003)
15. A.I. Buzdin, A.S. Mel'nikov, Phys. Rev. B **67**, 020503 (2003)
16. T.R. Kirkpatrick, D. Belitz, Phys. Rev. B **67**, 024515 (2003)
17. I.I. Mazin, D.J. Singh, Phys. Rev. B **69**, 020402 (2004)
18. M.D. Johannes, I.I. Mazin, D.J. Singh, D.A. Papaconstantopoulos, Phys. Rev. Lett. **93**, 097005 (2004)
19. T. Ishiguro, K. Tamaji, G. Saito, *Organic Superconductors*, 2nd edn. (Springer, 1998)
20. D. Jérôme, A. Mazaud, M. Ribault, K. Bechgaard, J. Phys. France Lett. **41**, L95 (1980)
21. D. Jérôme, Science **252**, 1509 (1991)
22. I.J. Lee, M.J. Naughton, G.M. Danner, P.M. Chaikin, Phys. Rev. Lett. **78**, 3555 (1997); S. Belin, K. Behnia, Phys. Rev. Lett. **79**, 2125 (1997); I.J. Lee, S.E. Brown, W.G. Klark, M.J. Strouse, M.J. Naughton, W. Kang, P.M. Chaikin, Phys. Rev. Lett. **88**, 017004 (2002); I.J. Lee, D.S. Show, W.G. Klark, M.J. Strouse, M.J. Naughton, P.M. Chaikin, S.E. Brown, Phys. Rev. B **68**, 092510 (2003)
23. A.G. Lebed, K. Machida, M. Ozaki, Phys. Rev. B **62**, R795 (2000)
24. K. Kuroki, R. Arita, H. Aoki, Phys. Rev. B **63**, 094509 (2001)
25. Y. Suginishi, H. Shimahara, J. Phys. Soc. Jpn **73**, 3121 (2004)
26. Y. Tanaka, K. Kuroki, Phys. Rev. B **70**, 060502 (R) (2004)
27. K. Kuroki, Y. Tanaka, T. Kimura, R. Arita, Phys. Rev. B **69**, 214511 (2004)
28. Y. Fuseya, Y. Suzumura, J. Phys. Jpn **74**, 1263 (2005)
29. Y. Ohta, S. Nishimoto, T. Shirakawa, Y. Yamaguchi, Phys. Rev. B **72**, 012503 (2005)
30. G.I. Japaridze, E. Müller-Hartmann, Phys. Rev. B **61**, 9019 (2000)
31. C. Dziurzik, G.I. Japaridze, A. Schadschneider, J. Zittartz, Eur. Phys. J. B **37**, 453 (2004)
32. A.O. Gogolin, A.A. Nersesyan, A.M. Tsvelik, *Bosonization and strongly correlated systems* (Cambridge University Press, 1998)
33. J.M. Kosterlitz, D.J. Thouless, J. Phys. C **11**, 1583 (1973)
34. P. Wiegmann, J. Phys. C **11**, 1583 (1978)
35. K.A. Muttalib, V.J. Emery, Phys. Rev. Lett. **57**, 1370 (1986); T. Giamarchi, H.J. Schulz, J. Phys. France **49**, 819 (1988); T. Giamarchi, H.J. Schulz, Phys. Rev. B **33**, 2066 (1986)
36. C.N. Yang, Phys. Rev. Lett. **63**, 2144 (1989).
37. S.R. White, Phys. Rev. Lett. **69**, 2863 (1992); S.R. White, Phys. Rev. B **48**, 10345 (1993)
38. *Density-Matrix Renormalization*, edited by I. Peschel, X. Wang, M. Kaulke, K. Hallberg (Springer, 1999)
39. U. Schollwöck, Rev. Mod. Phys. **77**, 259 (2005)